

COVER PAGE

Document downloaded by @DAEL

Sat Nov 28 07:27:49 2026
For personal use

When automatic English translation is provided, only the original document is authentic.
The EAA cannot be held responsible of any translation error

Bibliographical reference

Extension of Double Porosity Model to Porous Materials Containing Specific Porous Inclusions, Emmanuel Gourdon and Marco Seppi, Acta Acustica **vol. 96** (Number 2), 2010, pp. 275-291

DOI
https://doi.org/10.3813/AAA.918277

ACTA ACUSTICA UNITED WITH ACUSTICA
Vol. 96 (2010) 275 – 291

DOI 10.3813/AAA.918277

Extension of Double Porosity Model to Porous Materials Containing Specific Porous Inclusions

Emmanuel Gourdon[1)], Marco Seppi[2)]

[1)] Département Génie Civil et Bâtiment FRE CNRS 3237, Ecole Nationale des Travaux Publics de l'Etat, Membre de Université de Lyon, 69518 Vaulx en Velin Cedex, France. emmanuel.gourdon@entpe.fr

[2)] Imamoter Institute of the National Research Council of Italy (C.N.R.), 44100 Cassana, Italy. m.seppi@imamoter.cnr.it

Summary

Acoustical porous materials containing specific porous inclusions are studied. An extension of double porosity model based on the homogenization hypotheses introduced by Boutin [1] is presented. To apply and extend Olny's model [2, 3], some hypotheses together with the identification of the different regimes rely directly on the nature of the inclusion must be respected that is why the filling material is chosen to respect those assumptions (for example high contrast of permeability,...). The inclusions are supposed periodic and the frame rigid. The idea here is to use the diffusion effect already observed in double porosity case and to add poro-elastic inclusions to deal with the main disadvantage of double porosity case, i.e the presence of an hole. This hole leads to bad absorption bahavior at very low frequency and loss of performances in transmission. Experimental verifications are given by using different Kundt tubes. The semi-phenomenological model is thus validated.

PACS no. 43.55.Ev

1. Introduction

Porous materials are widely used in acoustics to improve the sound absorption coefficient. Perforations in the thickness direction can be made to increase the sound absorption coefficient of these materials. It creates double porosity into the material. This double porosity concept has been studied by several authors [1, 2, 4, 3, 5]. Thus, theoretical aspects have been investigated [1, 2, 3]. Numerical aspects and practical applications have also been studied [4, 5] and have shown that, under certain conditions, it is possible to enhance considerably the sound absorption coefficient.

Indeed, the acoustical sound absorption of double porosity materials can be larger than simple porosity materials: it depends strongly on the permeability of the porous substrate, on the material thickness and on the frequency range. Owing to this concept, new absorpbing materials can be designed to decrease the noise in the low frequency range [6, 7, 8]. However, the increase of absorption is usually obtained above a certain frequency value. At very low frequency, the sound absorption coefficient of a double porosity material decreases compared with the sound absorption coefficient of a single porosity material. Moreover, due to perforations, there is a loss of performances in transmission. This last problem can be important when a complex field is involved [9].

Received 6 May 2009,
accepted 15 January 2010.

In [3], it has been underlined that, in the case of double porosity and when the permeability contrast is high, a pressure diffusion effect can be observed. In this case, the absorption coefficient is increased significantly in a range around a theoretical frequency, called the diffusion frequency.

As described by Horoshenkov in [10], there is growing interest in innovative solutions concerning materials for acoustical applications. Moreover, inhomogeneous materials have been considered in [11, 12]. In particular, a study about porous heterogeneous acoustic materials made up of inclusions in the thickness direction, has been addressed by Groby et al. [13], concerning the case of inclusions in a periodical slab. In [13], a theoretical model for the pressure field equations based on the Green's functions is described and is followed by experimental verifications. The explored frequency range is very wide and comprehensive of the typical ultrasound frequencies. In our case, the range of interest is tuned for the typical acoustical applications ($50 - 4000$ Hz, or narrowed to $50 - 500$ Hz for some applications); moreover, the theoretical model is based on the homogenization hypotheses introduced by Boutin et al. [1].

The aim of the present study is to show that it is possible to use the pressure diffusion effect already observed in the double porosity case and to add poro-elastic inclusions into the perforations to deal with the main disadvantages of double porosity materials, i.e. loss of performances in transmission and very poor performances at very low frequencies. Semi-phenomenological model and

© S. Hirzel Verlag · EAA

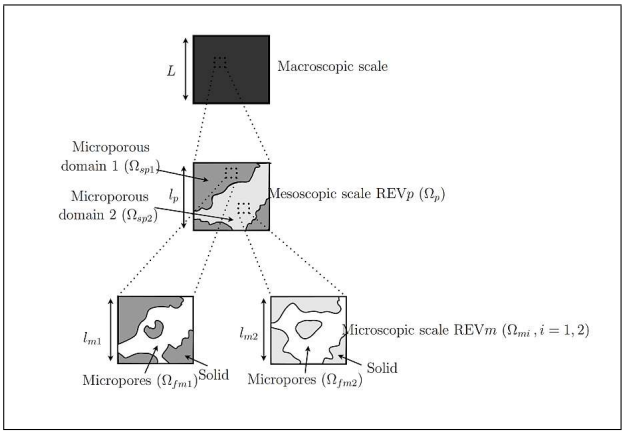


Figure 1. The three scales of the considered heterogeneous medium.

experimental results for the case of absorption are shown in the present paper. An example confirming the positive effect of inclusions in the case of transmission is also presented; this topic will be addressed extensively in forthcoming papers.

In the case of double porosity, the pressure diffusion effect is obtained through a highly resistive microporous material. In fact, such a characteristic provides a large difference between the resistivity of the microporous material and the resistivity of the air in the pores, that can be approximated to zero. As shown in [14] the same effect can be reproduced in the case of specific porous inclusions filling the holes, through a high difference in the air flow resistivity between the two involved microporous materials.

To apply and extend Olny's model [2, 3], some hypotheses together with the identification of the different regimes rely directly on the nature of the inclusion must be respected that is why the filling material is chosen to respect those assumptions (for example high contrast of permeability,...).

The paper is organized in the following way. Section 2 describes the semi-phenomenological model which is an extension of double porosity model and points out the acoustical and geometrical characteristics, that are necessary to obtain the supposed effects of sound absorption increase and pressure diffusion. Section 3 describes experimental results and model validation.

2. Semi-phenomenological model

Consider an heterogeneous medium composed of two poroelastic materials. Three scales are needed to describe the structure (Figure 1).

In what follows, it is assumed that there is a high permeability contrast between the two microporous domain 1 and 2. In all this study, we assume that the microporous domain 1 has a higher resistivity than the poroelastic inclusion (microporous domain 2) to obtain permeability contrast necessary for the increase of absorption.

Let $L, l_p, l_{mi},\ i = 1, 2,$ be, respectively, the three characteristic sizes for each level of representation: macroscopic, mesoscopic, and microscopic. In concrete terms, l_m and l_p are respectively given by the order of magnitude of the micro- and mesoheterogeneities, whereas the wavelength in the heterogeneous material can be used to evaluate L. It should be underlined that for double porosity material an estimate of this wavelength is provided by the wavelength in the pores. To obtain a separation of scales between meso and macro scales, one should have the ratio l_p/L small. Indeed, the meso-heterogeneities must be small compared with the macroscale to apply homogeneization. So, as the poro-elastic inclusion represents an heterogeneity, the le ngth L is chosen as the double porosity case (the meso-heterogeneity is now the inclusion). In what follows, the subscripts p, m, h are used to distinguish variables, respectively, related to poroelastic inclusions, micopores, and to the heterogeneous medium. In this system, one assumes the existence of two representative elementary volumes REVm and REVp defined, respectively, from the micropores and poroelastic inclusions structures. Poroelastic inclusions and micropores are supposed to be air-filled, and interconnected. Let ϕ_{m1} and ϕ_{m2} be respectively the porosity of material 1 and the porosity of material 2. The porosity of the heterogeneous medium ϕ_h can be written in function of porosities related to poroelastic inclusions and micropores (see Figure 1 for the definition of the terms),

$$\begin{aligned}\phi_h &= \frac{\Omega_{fm1}}{\Omega_{m1}}\frac{\Omega_{sp1}}{\Omega_p} + \frac{\Omega_{fm2}}{\Omega_{m2}}\frac{\Omega_{sp2}}{\Omega_p} \\ &= \big(1-\phi_p\big)\phi_{m1} + \phi_p\phi_{m2},\end{aligned} \tag{1}$$

where ϕ_p denotes the porosity to the fictive medium consisting of the microporous domain 1 mesoperforated with air where the microporous domain 2 (poroelastic inclusion) has been replaced by air. In order to represent the multiscale heterogeneous medium as a homogeneous equivalent one, the first assumption [3] that has to be made is that the characteristic size of the phenomenon is large compared with the "largest" heterogeneities. So a first separation of scales (macro/meso) must exist,

$$\frac{l_p}{L} \ll 1. \tag{2}$$

Moreover, a separation of scales between micro- and mesoscales must also exist [3],

$$\frac{l_{m1}}{l_p} \ll 1, \quad \frac{l_{m2}}{l_p} \ll 1. \tag{3}$$

A semi-phenomenological model of the wave propagation at audible frequencies is presented in the case where (i) the medium is periodic, (ii) there is a double separation of scales between micro and meso size on the one hand and between meso and macro size on the other hand, (iii) the motion of the skeleton can be neglected. In what follows, a temporal dependency $e^{j\omega t}$ is assumed.

The considered periodic cells are represented in Figure 2. They consist in a heterogeneous material. Indeed, a poroelastic inclusion is considered. In the case in which the poroelastic inclusion is air Olny et al. [2, 3] established

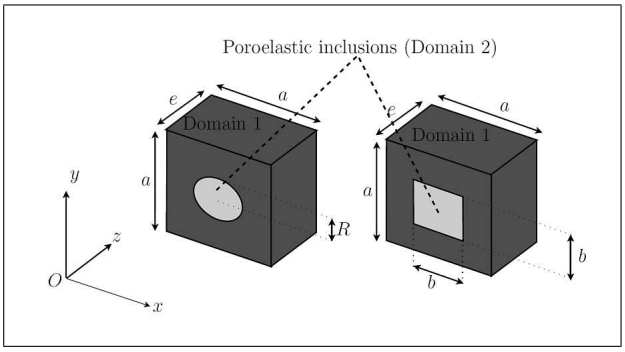


Figure 2. Considered periodic cells: circular or square cross-section for the poroelastic inclusion.

a generalized Darcy's law similar to single porosity media involving a dynamic permeability Π_{dp} and a bulk modulus K_{dp} depending on the mesogeometry.

If one is interested in the propagation in the direction parallel to the axis z, similarly to what has been done in [2, 3], the characteristic impedance Z_c and the propagation constant k in the heterogeneous medium can be determined with homogeneization by

$$Z_c = \sqrt{\rho_h K_h} \quad \text{and} \quad k = \omega\sqrt{\frac{\rho_h}{K_h}}, \tag{4}$$

where the effective density ρ_h is related to the dynamic permeability Π_h by

$$\rho_h = \frac{\eta}{\mathrm{j}\omega\Pi_h}, \tag{5}$$

where η denotes the dynamic viscosity of the interstitial fluid. The surface impedance Z_h of a material of thickness e and backed by a material of surface impedance Z_S can then easily calculated by

$$Z_h = Z_c\frac{Z_c - \mathrm{j}Z_S\cot(ke)}{Z_S - \mathrm{j}Z_c\cot(ke)}. \tag{6}$$

The normal incidence sound absorption coefficient is then given by

$$\alpha = \frac{4Real[z_h]}{(Real[z_h]+1)^2 + Imag[z_h]^2} \tag{7}$$

with $z_h = Z_h/(\rho_a c_a)$, where ρ_a and c_a are the density and sound speed in the medium in which the incident wave propagates.

Visco-inertial effects and thermal effects are modelized by using a direct extension of Olny's model to porous materials containing porous inclusions by considering that the meso-pores of the double porosity material are filled here with a porous material. Indeed, we modify the expressions of the viscous and thermal permeabilities based on the substitution of pores variables with porous inclusion variables under the hypotheses that the Olny's model [2, 3] assumptions are respected. Those assumptions can be respected by choosing a specific filling material.

For visco-inertial effects, the materials are considered in parallel and for thermal effects we add a diffusion function to take into account the diffusion effects. It should be underlined that, to apply and extend Olny's model [2, 3], some hypotheses together with the identification of the different regimes rely directly on the nature of the inclusion that is why in the following the filling material is chosen to respect those assumptions (for example high contrast of permeability,...). The authors have checked carefully those different assumptions to be sure to be able to extend the Olny's model in this particular case. This last point has not be detailed here because it is just necessary to follow publication [3]. Further discussions and details about the model which has to be taken for any porous inclusion will be given in another paper.

2.1. Visco-inertial effects

Similarly to [2, 3], in the case of circular cylindrical inclusions of poroelastic inclusions, the dynamic permeability Π_h of the whole heterogeneous material in the direction normal to the material is given by

$$\Pi_h = (1-\phi_p)\Pi_{m1} + \phi_p\Pi_{m2} \tag{8}$$

where Π_{mi} , $i = 1, 2$, denotes the dynamic permeability of the single porosity microporous medium i.

An approach based on a semiphenomenological model is chosen for the calculation of each Π_{mi} , $i = 1, 2$. This approach consists in using the acoustical parameters of the Johnson et al's semiphenomenological model [15] (ϕ_{mi}, σ_{mi} the micro-resistivity, $\alpha_{\infty mi}$ the tortuosity and Λ_{mi} the viscous characteristic length , $i = 1, 2$). Thus, the dynamical permeability of each microporous domain is [15]:

$$\Pi_{mi}(\omega) = \frac{\Pi_{mi}(0)}{\mathrm{j}\frac{\omega}{\omega_{vmi}} + \sqrt{1 + \mathrm{j}\frac{M_{mi}}{2}\frac{\omega}{\omega_{vmi}}}}, \quad i = 1, 2 \tag{9}$$

where $\Pi_{mi}(0)$ is the static permeability of the i-th single porosity medium, given by $\Pi_{mi}(0) = \eta/\sigma_{mi}$,

$$\omega_{vmi} = \sigma_{mi}\phi_{mi}/(\rho_0\alpha_{\infty mi}) \tag{10}$$

denotes the viscous characteristic frequency of the i-th microporous medium and $M_{mi} = 8\alpha_{\infty mi}\eta/\ (\phi_{mi}\sigma_{mi}\Lambda_{mi}^2)$ and ρ_0 is the static air density.

2.2. Thermal effects

Similarly to [2, 3], in the case of circular cylindrical inclusions of poroelastic inclusions and for high permeability contrast between the two microporous domain 1 and 2, the macroscopic dynamical bulk modulus K_h can be given by

$$K_h = \left[\frac{\phi_p}{K_{m2}(\omega)} + (1-\phi_p)\frac{F_d(\omega)}{K_{m1}(\omega)}\right]^{-1}. \tag{11}$$

K_{m1} and K_{m2} are respectively the dynamical bulk moduli of the single porosity domain 1 and the single porosity domain 2.

An approach based on a semiphenomenological model is chosen for the calculation of K_{mi}, $i = 1, 2$. Several approaches are possible. The first one consists in using the acoustical parameters of the Champoux-Allard's semiphenomenological model [16] (ϕ_{mi} and Λ'_{mi} the thermal characteristic length). Thus, the dynamical bulk modulus of the microporous domains are [16]

$$K_{mi}(\omega) = \frac{\gamma P_0/\phi_{mi}}{\gamma - (\gamma-1)\left[1 - \mathrm{j}\frac{8\kappa}{\Lambda'^2_{mi} C_p \rho_0 \omega}\sqrt{1 + \mathrm{j}\frac{\Lambda'^2_{mi} C_p \rho_0 \omega}{16\kappa}}\right]^{-1}} \quad (12)$$

C_p denotes the specific heat at constant pressure, γ the ratio of the specific heats and κ the conductivity of the air.

A second approach (that is used in the present paper) consists in using the acoustical parameters of the Champoux-Allard-Lafarge semiphenomenological model [17] (ϕ_{mi}, Λ'_{mi} and $\Theta_{mi}(0)$). In this case, the dynamical bulk modulus of the microporous domains are [17]

$$K_{mi}(\omega) = \frac{\gamma P_0/\phi_{mi}}{\gamma - j(\gamma-1)\frac{\Theta_{mi}}{\delta_t^2 \phi_{mi}}}, \quad (13)$$

where P_0 is the static ambient pressure, $\delta_t = \sqrt{\kappa/(\rho_0 C_p \omega)}$ is the thermal boundary layer thickness and Θ_{mi} denotes the dynamic thermal permeability of the i-th microporous domain, that can be computed as

$$\Theta_{mi}(\omega) = \frac{\Theta_{mi}(0)}{\mathrm{j}\frac{\omega}{\omega_{tmi}} + \sqrt{1 + \mathrm{j}\frac{M'_{mi}}{2}\frac{\omega}{\omega_{tmi}}}}, \quad i = 1, 2, \quad (14)$$

where

$$\omega_{tmi} = \kappa \phi_{mi}/(\rho_0 C_p \Theta_{mi}(0)) \quad (15)$$

denotes the thermal characteristic frequency of the i-th microporous domain and $M'_{mi} = 8\Theta_{mi}(0)/(\phi_{mi}\Lambda'^2_{mi})$.

F_d is the ratio of the average pressure in the micropores to the pressure in the poroelastic inclusion. This function describes the pressure diffusion effects occurring when the wavelength in the porous domain becomes of the same order of magnitude as the size of meso-heterogeneities (the size l_p). This function is associated with a characteristic frequency

$$\omega_d = \frac{(1-\phi_p)P_0}{\phi_{m1}\sigma_{m1} D(0)}, \quad (16)$$

where $D(0)$ can be estimated by [3]

$$D(0) \simeq (1-\phi_p) l_p^2, \quad (17)$$

with l_p the size of the meso-heterogeneities ($l_p = 2R$ for circular cross-section or $l_p = b$ for square cross section).

- For frequencies such that $\omega \ll \omega_d$, F_d tends to 1 as ω decreases, the pressure is uniform in the whole material [3]. Thus, no pressure diffusion effect occurs and it is sufficient to replacing F_d by 1 in Equation (11).
- For frequencies such that $\omega \gg \omega_d$, F_d tends to 0 as ω increases: the micro-pores do not participate in the macroscopic response of the material [3].
- For frequencies around ω_d, F_d is complex and describes dissipation effects specific to multi-scales porous materials: the pressure diffusion effects [1, 3].

So, for frequencies such that $\omega \sim \omega_d$, the pressure in the micro and mesoscopic domains are of the same order of magnitude but differ.

In a first approximation, we apply and extend Olny's model [2, 3]: we consider that the filling material is chosen to respect the assumptions of the Olny's model (for example high contrast of permeability). We consider that there is a high contrast permeability which ensures that diffusion process will appear exactly as the double porosity case. The resistivity of the filling material is much smaller than the resistivity of the porous domain 1. For diffusion, everything happens as if the same phenomenon of diffusion appears: the contrast of permeability is high so it is as if for diffusion phenomenon the meso-heterogeneity represents a hole. The authors are aware that it is an approximation which is not exact since F_d is the ratio of the average pressure in the micropores to the pressure in the porous inclusions but for specific filling materials the physics appears to be quite similar that is why the authors have chosen this approximation. The authors have checked that by using a specific filling material, the assumptions of Olny's model are respected. Further discussions and details about the diffusion function which has to be taken for any porous inclusion will be given in another paper.

So, when the dissipative effects of pressure diffusion occur, F_d can take the form [3]

$$F_d(\omega) = 1 - \mathrm{j}\frac{\omega}{\omega_d}\frac{D(\omega)}{D(0)}, \quad (18)$$

where $D(\omega)$ is a function whose properties can be compared with the ones of the thermal permeability introduced by Lafarge et al [17]. It is associated with the pressure diffusion effects [2, 3] which can occur in the heterogeneous material depending on its physical properties (high permeability contrast necessary) and frequency. Those effects arise through a variation of the pressure in the micropores at the mesoscopic scale and an increase of the imaginary part of the macroscopic bulk modulus of the material thereby inducing a dramatic increase of the sound absorption. A semi-phenomenological expression of $D(\omega)$ is [3] given by

$$D(\omega) = \frac{D(0)}{\mathrm{j}\frac{\omega}{\omega_d} + \sqrt{1 + \mathrm{j}\frac{M_d}{2}\frac{\omega}{\omega_d}}} \quad (19)$$

and the static value of D, $D(0)$, is a geometric parameter.

The form parameter M_d introduced in Equation (19) is

$$M_d = \frac{8D(0)}{\Lambda_d^2(1-\phi_p)}, \quad (20)$$

where

$$\Lambda_d = 2\frac{\Omega_{sp1}}{\partial\Omega_{sp1}}. \tag{21}$$

Ω_{sp1} refers to the part of the mesoscopic representative elementary volume occupied by the microporous domain 1 and $\partial\Omega_{sp1}$ is the area of the interface between the microporous domain 1 and the microporous domain 2 in the mesoscopic representative elementary volume. So for straight circular cross-section,

$$\Lambda_d = \frac{a^2 - \pi R^2}{\pi R}. \tag{22}$$

As discussed in [2], for finite thickness materials, the theoretical model must be corrected so that the surface $\partial\Omega_{sp1}$ should also include the surface of the microporous domain in contact with the exterior air when the heterogeneous material is backed by a rigid wall. With this thickness correction, for rigid wall termination

$$\Lambda_d = \frac{2e(a^2 - \pi R^2)}{2e\pi R + (a^2 - \pi R^2)} \tag{23}$$

For a circular cross-section, the geometric parameter $D(0)$ can be evaluated analytically [5, 18]

$$D(0) = \frac{a^2}{4\pi}\left(\ln\left(\frac{1}{\phi_p}\right) - \frac{3}{2} + 2\phi_p - \frac{\phi_p^2}{2}\right), \tag{24}$$

with $\phi_p = \pi R^2/a^2$ where a is the size of the cell (Figure 2).

When only one layer is considered (independently from its nature, double porosity or heterogeneous material), the surface impedance Z_S in equation (6) can be considered infinite. Thus equation (6) is reduced to

$$Z_h = -\mathrm{j}Z_C\cot(ke). \tag{25}$$

When several layers are considered, equation (25) has to be used for the first layer, backed by a rigid wall. When other layers are added side by side, for each new layer equation (6) has to be recalculated to obtain the new surface impedance for the layer, until the last external layer. With this method, a multi-layer porous material characterized by a number of layers as large as wanted can be calculated.

Thus, for the coupling between a double porosity material layer and a heterogeneous or single porosity material, the whole can be treated like a multi-layer porous material. The calculation of Λ_d, M_d and all the parameters associated with double porosity or heterogeneous material, is done for each layer. It should be underlined that the diffusion surface corresponds to the interface surface between the microporous domain 1 and the air or the small resistive micro-porous domain 2. For example, with the hybrid configuration shown in Figure 3, the surface of diffusion to take into account for the first layer is $\partial\Omega_1$ (double porosity), and $\partial\Omega_2$ for the second layer (melamine inclusion). In the case where the two layers present a high contrast of permeability, the surface $\partial\Omega_3$ has to be taken into account. The surface between melamine and air has not to be taken into account since the permeability contrast is not high. Then impedance calculations at each interface from an extremity of the multi-layer porous material to another allow to calculate the acoustical properties.

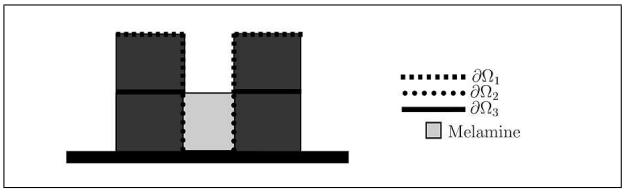


Figure 3. Example of a hybrid configuration with a multi-layer porous material.

3. Experimental results and model validation

In this Section, experimental verifications are presented. The heterogeneous case is the main issue of the present study. The case of double porosity is used as a reference. In fact, the performance of the heterogeneous material is compared with the performance of the double porosity configuration.

3.1. Materials and testing

A consistent number of experimental data and analytical calculations will be presented and compared in following sections.

3.1.1. Materials choice

The materials initially used are named u160 and melamine. The first one is a foam composed of recycled materials, the second one is a well-known white melamine. White melamine is used for inclusions and u160 is used for supporting material. Their properties have been experimentally characterized in the Entpe Labs and are presented in Table I. ϕ is experimentally measured as described in [19]. The resistivity σ is experimentally measured using the standard method ASTM [20]. α_∞, Λ, Λ' and $\Theta(0)$ have been indirectly determined by using analytical formulas [21] deduced from Johnson-Champoux-Allard models [15, 16] or Johnson-Champoux-Allard-Lafarge [17]. ρ_1 has been classically measured. For E, ν and η_S, the resonant mass-spring method has been used. The method is based on the measurement of frequency response of rectangular sample linked to a vibrating support. A metalic plate of mass M is fixed on the top of the sample to obtain the resonant mass-spring system. Different shape factors are used. Analysis of the frequency responses leads to the damping coefficient and to an apparent Young modulus. The true Young modulus is linked to the apparent Young modulus by a multiplicative coefficient which depends on the shape of the sample and on the Poisson ratio. For a given shape factor, this correction coefficient depends only on ratio Poisson [22].

Table I. Material properties.

Material	ϕ	$\sigma(N\,s\,m^{-4})$	α_∞	$\Lambda\,(m)$	$\Lambda'\,(m)$	$\Theta(0)\,(m^2)$	$\rho_1\,(kg\,m^{-3})$	$E\,(kPa)$	ν	η_s
u160	0.90	47700	1.29	24×10^{-6}	200×10^{-6}	2.9×10^{-9}	159.8	500	0.4	0.180
melamine	0.99	10000	1.00	100×10^{-6}	200×10^{-6}	3.3×10^{-9}	8.5	235	0.3	0.066
rockwool	0.97	50000	1.07	175×10^{-6}	175×10^{-6}	3.3×10^{-9}	130	4400	0	0.1

The two materials have been chosen for the following reasons:

- high resistivity contrast between the two materials allow to satisfy the hypotheses on which the double porosity model is based on;
- u160 is a good absorbing material and inclusions of melamine can improve its performances at low frequencies.

In addition, the microporous u160 is a good candidate, that respects the condition of flow viscosity [5] in the measured frequency domain (approximatively under 4500 Hz).

In fact, from equation (10), ω_{vm} = 27733rad/s, therefore in the range $\omega < \omega_{vm}$ and the flow can be considered viscous. From a theoretical point of view, the possibility to obtain an absorption gain due to pressure diffusion mechanisms is effective.

Moreover, a second microporous material acting as a frame in the heterogeneous configuration, has been used for verification. It is a common rockwool and is here referred just as rockwool.

3.1.2. Testing instruments

The testing instruments used for the measurements of sound absorption consisted of

- a custom built standing wave tube (here named Small Kundt Tube, SKT - Figure 4), having a circular cross-section of a 46mm diameter, on which two microphone positions are available on the top of the tube in front of the sample and one on the back. In this way, both absorption and dynamic density / bulk modulus measurements are possible, in a range approximately between 150 and 4300 Hz;
- a B&K type 4106 standing wave tube (here named Medium Kundt Tube, MKT - Figure 5), having a circular cross-section of a 100 mm diameter, on which four microphone positions are available on the top of the tube. In this way, both absorption and transmission measurements are possible. For absorption, the available frequency range falls approximately between 150 and 2000 Hz; topics about transmission will be discussed in a further paper;
- an home made 5.5m long standing wave tube (here named Big Kundt Tube, BKT - Figure 6), having a square cross-section of 600 mm × 600 mm. Two peculiarities of the BKT are important for the present study: the measurable frequency range, that comprehends low frequencies (approximately between 50 and 500 Hz), and the dimension of the cross-section, that permits an investigation of samples characterized by series of periodical cells. More details about the ENTPE big standing wave tube can be found in [23], p. 77-80 and in [2].



Figure 4. Small Kundt Tube. Left: front view, right: top view.

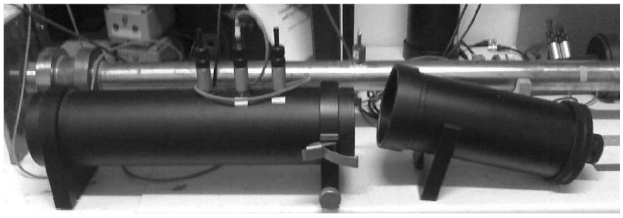


Figure 5. Medium Kundt Tube.

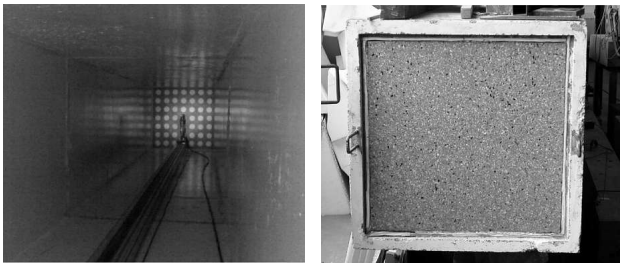


Figure 6. Big Kundt Tube. Left: rail and microphone in the interior, right: preparation of a sample of u160.

3.2. Experimental results

In this section, the results of the experimental measurements are presented. Two configurations have been tested,

- double porosity, with u160 as microporous material;
- heterogeneous, with u160 as main microporous material filled up by melamine as inclusion.

The heterogeneous case is the main issue of the present study. The case of double porosity is used as a reference. In fact, the performance of the heterogeneous material is here compared with the performance of the double porosity configuration. Moreover, the semi-phenomenological model is first verified through comparison with the experimental results in the case of double porosity. As a second

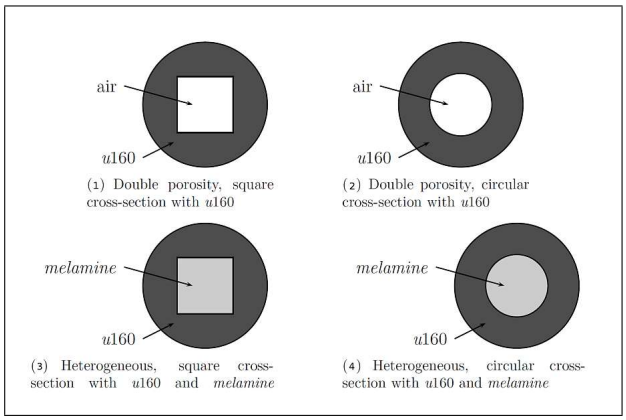


Figure 7. Sketch of cross-section geometries for a sample in the SKT or in the MKT, representing a single cell.

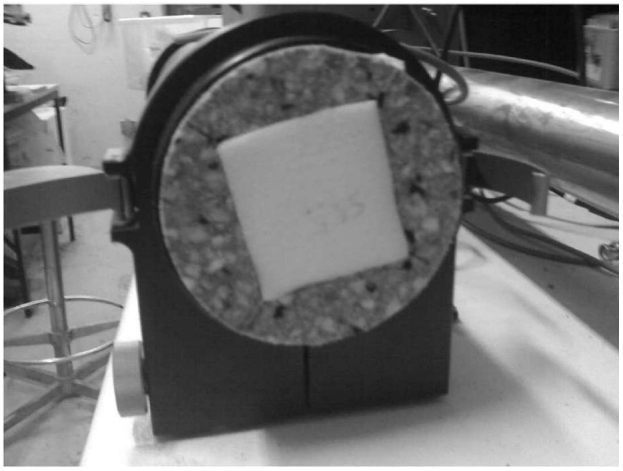


Figure 8. Example of an heterogeneous sample (u160 - melamine) in the Medium Kundt Tube.

step, the semi-phenomenological model and the comparison are extended to the heterogeneous case. The first experimental tests were performed in the Small and Medium Kundt Tubes. In those cases the external cross section of the sample is circular and only one periodic cell can be considered (Figure 7), due to the small dimensions and geometry of the sample. Therefore, the hypotheses of the homogenization theory are not completely satisfied, however this simple configuration was first a good approximation of a larger layer. The effect of different sized cross sections, i.e. the mesoporosity variation, have been tested but are not presented in the present paper. Indeed, the information obtained was useful to prepare the tests in the Big Kundt Tube, that require much more time for the preparation of the sample and for the measurement.

Experimental tests in the Big Kundt Tube are important to verify the validity of the homogenization theory [2, 3]. Only when a consistent number of cells is present, the theoretical hypotheses are valid. In the case of double porosity or heterogeneous materials with inclusions, the results obtained in the Small Kundt Tube for a single cell appears to be in good agreement compared with models

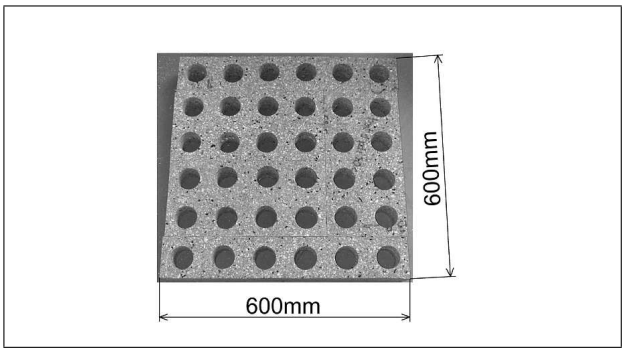


Figure 9. 90 mm thick u160 sample in the Big Kundt Tube: the frame.

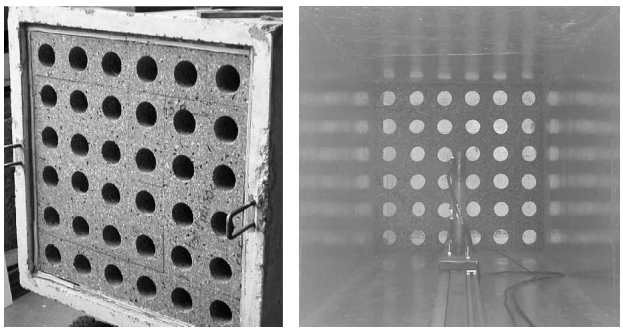


Figure 10. 90 mm thick double porosity (u160) sample in the Big Kundt Tube. Left: exterior view, right: interior view.

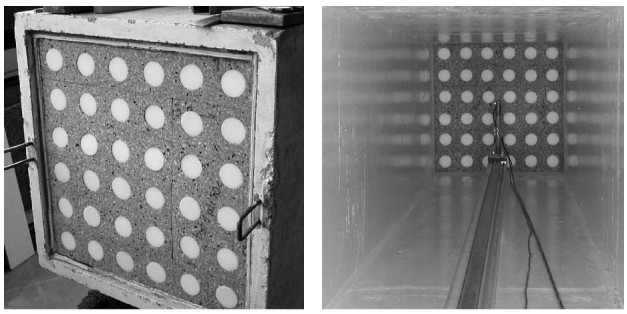


Figure 11. 90 mm thick heterogeneous (u160 - melamine) sample in the Big Kundt Tube. Left: exterior view, right: interior view.

but it should be verified that they are preserved in the passage from a single cell to a complete layer.

3.2.1. u160 as a frame material

The case with u160 as original microporous material to be filled with melamine is here presented.

The cross section of the Big Kundt Tube is a 600 mm × 600 mm square (see Table IV). The size of the cell (10 mm × 10 mm) has been chosen to have a similar aspect ratio if compared with the samples of the middle Kundt tube. The size of the perforation has been chosen among the tool sizes available. A radius of 29mm represents a good compromise in mesoporosity (0.264): large enough to permit the diffusion effects, but not too large to prevent losses at low frequency.

The measured absorption coefficients are presented in Figure 13. The small dips appearing in all the curves at

Table II. Small Kundt Tube geometries.

Configuration	External cross section		Internal cross section		Mesoporosity	Thickness
	Shape	Dimension (mm)	Shape	Dimension (mm)	(-)	(mm)
A	circular	$r = 23$	square	$l = 10$	0.060	45
B	circular	$r = 23$	square	$l = 14$	0.118	45
C	circular	$r = 23$	square	$l = 25$	0.376	45
D	circular	$r = 23$	circular	$r = 14.5$	0.397	45

Table III. Medium Kundt Tube geometries.

Configuration	External cross section		Internal cross section		Mesoporosity	Thickness
	Shape	Dimension (mm)	Shape	Dimension (mm)	(-)	(mm)
A	circular	$r = 50$	square	$l = 21$	0.056	45.5
B	circular	$r = 50$	square	$l = 30$	0.115	45.5
C	circular	$r = 50$	square	$l = 55.5$	0.392	45.5
D	circular	$r = 50$	circular	$r = 23$	0.212	45.5

Table IV. Big Kundt Tube geometry for the samples characterized by a frame of u160.

Number of cells	Cell external cross section		Cell internal cross section		Mesoporosity
	Shape	Dimension (mm)	Shape	Dimension (mm)	(-)
6×6	square	$l = 100$	circular	$r = 29$	0.264

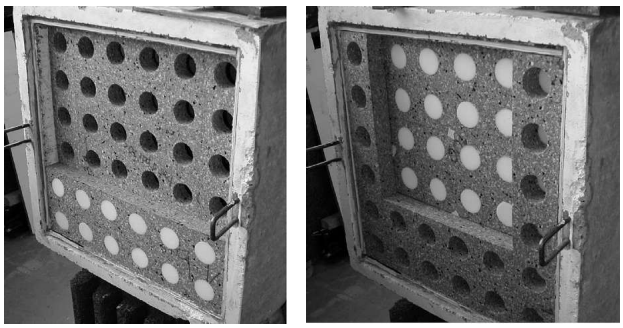


Figure 12. Preparation of the 90 mm thick heterogeneous (u160 - melamine) hybrid sample in the Big Kundt Tube. The material covers all the cross section (it is just for convenience and to better show the principle that the material does not cover all the cross section on the photography). Left: double porosity - heterogenous, right: heterogenous - double porosity.

the same frequencies, making them slightly discontinuous, can be explained by an internal problem in the acquisition card (it is not plate resonances). Indeed, after having checked every component of the experiment, it has been found that the acquisition card has a problem at those frequencies.

The results show the typical pattern for the double porosity curve, and a good improvement of the absorption coefficient for the heterogeneous material. In fact, above 350 Hz double porosity provides an higher absorption coefficient, but the inclusions permit a good improvement of the absorption coefficient if compared with double porosity at low frequency and almost no loss to the original u160 layer. In general, on a larger frequency range, the heterogeneous material shows the best performance.

The hybrid solutions, built up by placing side by side a double porosity 45 mm thick layer and an heterogeneous 45 mm thick layer, appear as an interesting compromise. In this case, the measured absorption coefiicients are between the double porosity and the heterogeneous case. The resulting curve is mainly driven by the first layer encountered by standing wave, but an improvement can be seen if compared with the original cases. As already pointed out, the optimization depends on the frequency target. For example, the hybrid configuration (a 45 mm thick double porosity layer in the front and a 45 mm thick u160 - melamine heterogeneous layer in the back) is better than the double porosity layer for the measured frequency range, but is still worse than the original u160 below 230 Hz. The vice versa configuration is very close to the regular heterogeneous solution: some absorption can be gained above 250 Hz, but there is a small loss below 200 Hz.

3.2.2. Rockwool as a frame material

The case with rockwool as original microporous material to be filled with melamine is here presented. With this material, two different mesoporosities have been investigated,

Table V. Big Kundt Tube geometry for the samples characterized by a frame of rockwool.

Number of cells	Cell external cross section		Cell internal cross section		Mesoporosity
	Shape	Dimension (mm)	Shape	Dimension (mm)	(-)
6×6	square	$l = 100.0$	circular	$r = 29$	0.264
7×7	square	$l = 85.7$	circular	$r = 29$	0.360

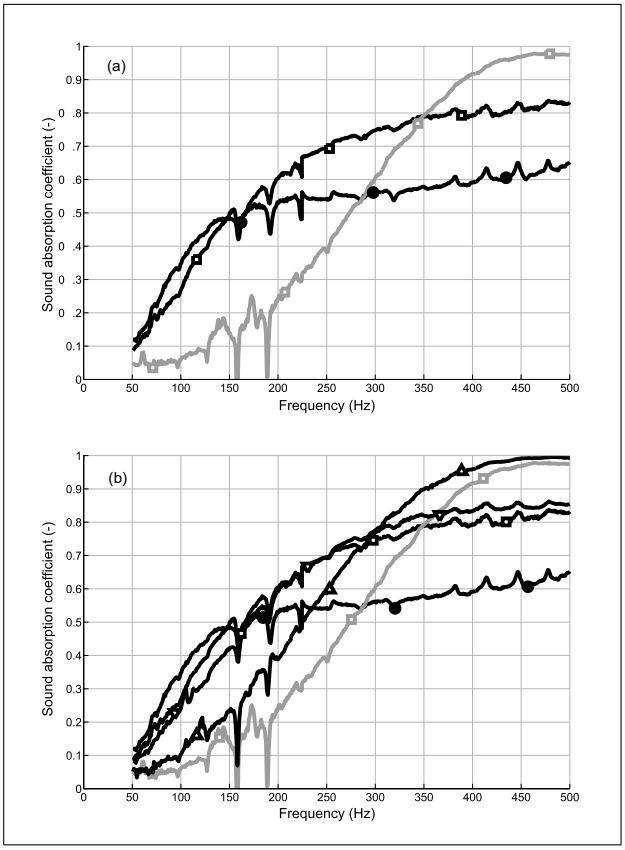


Figure 13. Big Kundt Tube, 90 mm thick layer, influence of the inclusions. (a) Cases of double porosity (grey square) and u160-melamine heterogeneous material (balck square), compared to the homogeneous u160 (black circle). (b) As in (a), with two hybrid solutions: a 45 mm thick double porosity layer in the front and a 45 mm thick thick u160-melamine heterogeneous layer in the back (black triangle) and the vice versa (inversed black triangle).

as resulting from a 90 mm thick sample characterized by a 6×6 or by a 7×7 periodical cells geometry (Table V and Figure 14). The results (Figure 15) show a similar behavior to the one observed for the case of u160: the typical pattern for the double porosity curve, and a good improvement in absorption for the heterogeneous material. It has also been shown that in the case of 7×7 holes (i.e. when mesoporosity is increased if compared with the case of 6×6 holes) the configuration is closer to an optimized solution in the frequency range 0-500 Hz. In fact, for these frequencies, the heterogenous curve is always above the double porosity one.

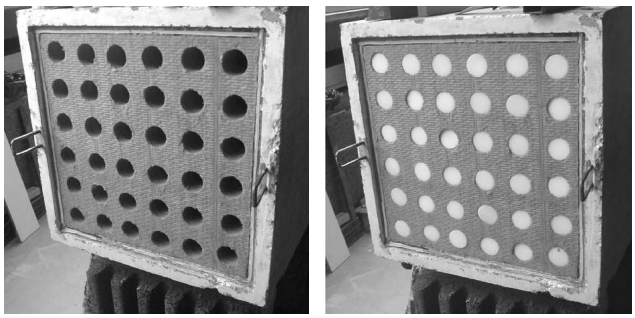


Figure 14. 90 mm thick 6×6 periodical cells rockwool sample in the Big Kundt Tube. Left: double porosity, right: heterogenous (with inclusions of melamine).

The hybrid solutions provide the same effects as discussed previously.

3.3. Validation of the semi-phenomenological model

In the following part, the semi-phenomenological model described previously is compared with the experimental data, for the measurements described above. The rigid frame Johnson-Lafarge model is used as base for the analytical prediction. The acoustical parameters (Johnson-Lafarge model) are presented in Table I. For the case of double porosity, the model described in [5] (from which the semi-phenomenological model described previously is derived) is used.

3.3.1. Periodical cells in the Big Kundt Tube

The model described previously has been used to predict the sound absorption coefficient for the configurations tested in the Big Kundt Tube, with u160 as microporous material acting as a frame. There is a good agreement between experimental data and prediction in Figure 16. The homogenization hypotheses of the semi-phenomenological model are represented with a good approximation in the experimental data by the presence of the 6×6 network of cells. The analytical calculation refers to the case of a circular-shaped inclusion into a square-shaped cell, as in Equation (24): the geometrical configuration (Table IV) is well represented. A thickness of 91 mm is considered instead of the 90 mm nominal thickness, due to tolerances and mounting conditions. The diffusion effect is taken into account by equation (18). For the case of double porosity the model described in [5] is taken into account; for the case of inclusions, the analytical equations can be found in previous part of the paper.

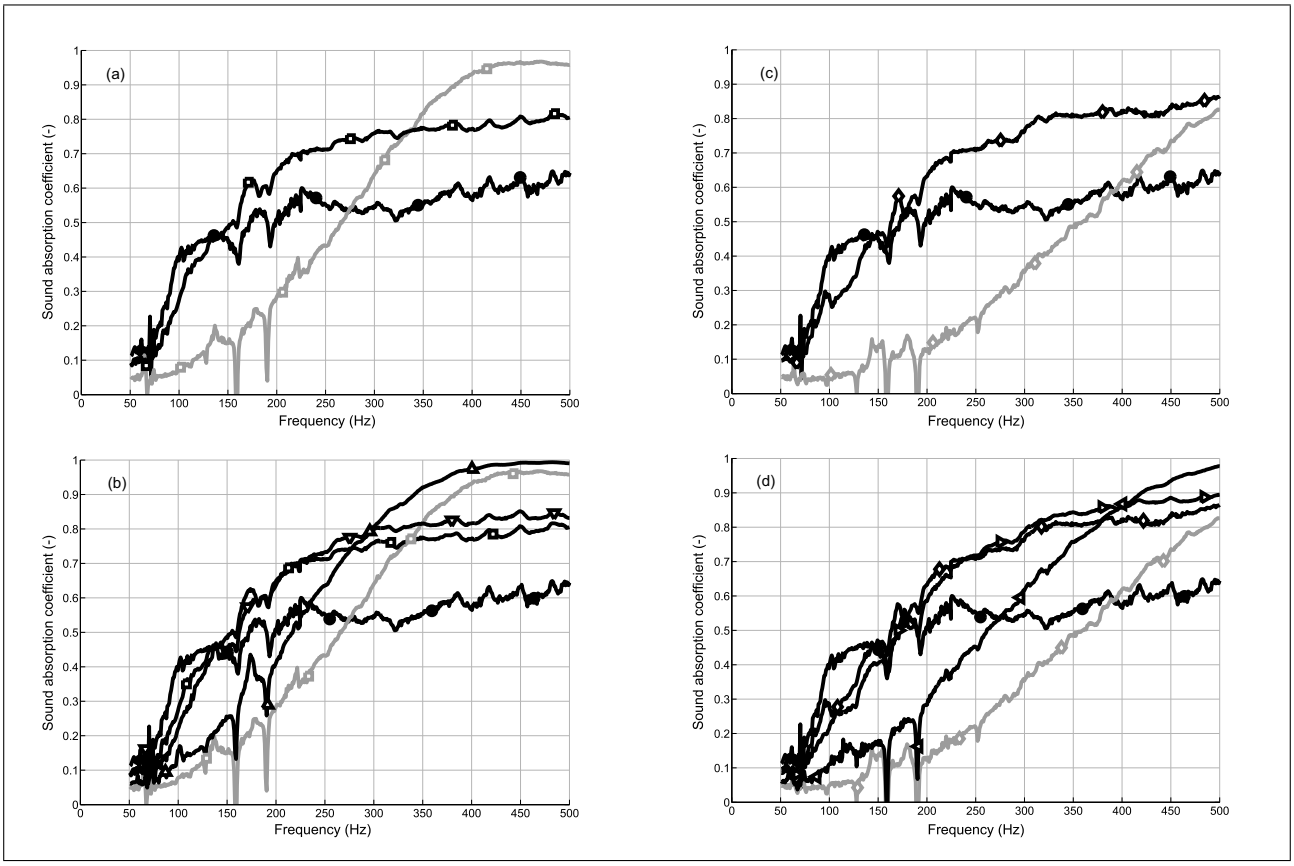


Figure 15. Big Kundt Tube, rockwool as frame microporous material, 90 mm thick layer: influence of the inclusions. (a) Configuration with 6 x 6 perforations, cases of double porosity (grey square) and rockwol-melamine heterogeneous material (black square) compared to the homogeneous rockwool (black circle). (b) As in (a), with two hybrid solutions: a 45 mm thick double porosity layer in the front and a 45 mm thick rockwool-melamine heterogeneous layer in the back (black triangle) and the vice versa (inversed black triangle). (c) Configuration with 7 x 7 perforations, cases of double porosity (grey diamond) and rockwol-melamine heterogeneous material (black diamond) compared to the homogeneous rockwool (black circle). (d) As in (c), with two hybrid solutions: a 45 mm thick double porosity layer in the front and a 45 mm thick rockwool-melamine heterogeneous layer in the back (black triangle -<-) and the vice versa (inversed black triangle ->-).

Hybrid solutions are thus considered (two layers are involved): the total impedance of a 90 mm thick hybrid layer is obtained by Equation (25) applied to the first 45 mm thick layer (for example double porosity layer in Figure 12a) and equation (6) for the second 45 mm thick layer (for example double porosity layer in Figure 12a). The small difference between the semi-phenomenological model and the experimental curves in Figure 16 can be ascribed to the axial tolerance of the perforations. In fact, some small misalignments are produced in practice, their effect being a small increase of the geometrical area that acts in the diffusion process and therefore a small increase of the sound absorption coefficient. In fact the diffusion surface will increase because for example the interface between microporous domain 1 and the air will increase. Discrepancies between semi-phenomenological model and experimental data can be explained by the way the coupling is handled in the formulation.

Moreover, eventual small gaps of air between the two layers due to tolerances during the mounting phase, in general do not deteriorate the absorption properties. Considering these two issues, the use of inclusions should result in a robust methodology also for practical applications. The intersections between predicted curves in Figure 16a are approximately at the same frequencies than the corresponding intersections between experimental curves: the semi-phenomenological model predicts well the frequency ranges when a configuration (double porosity, heterogeneous, etc.) is performing better than another one.

The good agreement already experienced for single layer configurations (Figure 16a) is confirmed for the hybrid configurations also: Figure 16b.

3.3.2. Single cell in the Small Kundt Tube

The analytical calculation refers to the case of a square-shaped (configurations A, B, C from Table II) or circular-shaped (configuration D in Table II) perforation or inclusion into a circular-shaped cell. The expression for $D(0)$ (equation (24) which is valid for a circular meso-heterogeneity into a square porous cell) must now be adapted. Equivalent areas are considered: the dimension a represents the size of a square whose area is the same as the one of the circular cross-section of the Tube.

Table VI. Homogenization conditions and static permeability contrast for the different tested samples.

Kundt Tube type	Configuration	Mesoporosity scale l_p (mm)	Interscale ratio l_m/l_p (-)	Permeability contrast	Diffusion frequency $f_d = \omega_d/2\pi$ (Hz)
Big Kundt Tube	6×6 cells	29.0	$6.9 \cdot 10^{-3}$	HIGH	1070
Small Kundt Tube	A	5.0	$8.0 \cdot 10^{-2}$	LOW	1868
Small Kundt Tube	B	7.0	$5.7 \cdot 10^{-2}$	LOW	2891
Small Kundt Tube	C	12.5	$3.2 \cdot 10^{-2}$	HIGH	11118
Small Kundt Tube	D	14.5	$2.8 \cdot 10^{-2}$	HIGH	12348
Medium Kundt Tube	A	10.5	$3.8 \cdot 10^{-2}$	LOW/HIGH	381
Medium Kundt Tube	B	15.0	$2.7 \cdot 10^{-2}$	LOW/HIGH	598
Medium Kundt Tube	C	27.8	$1.4 \cdot 10^{-2}$	HIGH	2546
Medium Kundt Tube	D	23.0	$1.7 \cdot 10^{-2}$	LOW/HIGH	1044

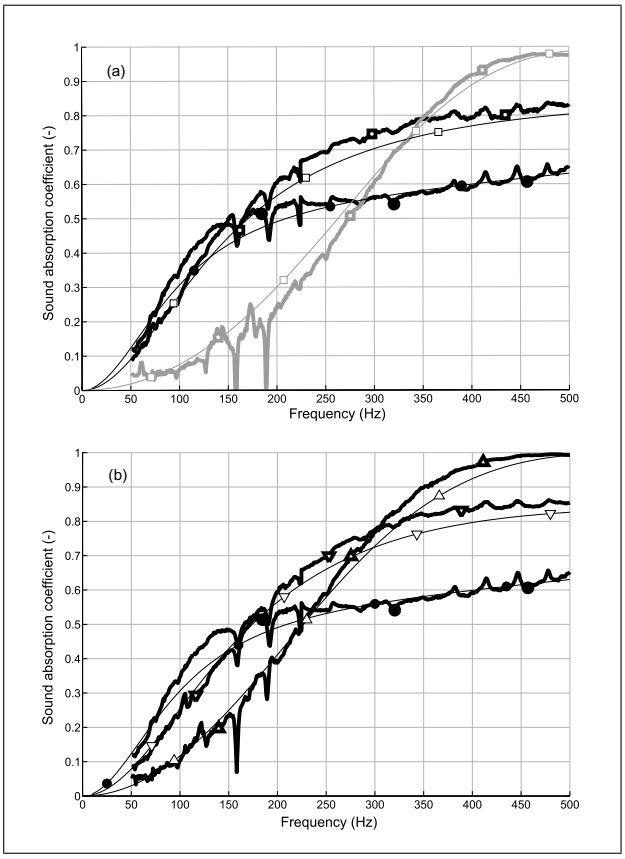


Figure 16. Big Kundt Tube, 90 mm thick layer composed of u160 and melamine, validation. (a) Comparison between experimental (solid line) and analytical (thin line) data: single porosity u160 (black circle), double porosity u160 (grey square), heterogeneous u160-melamine (black square). (b) Comparison between experimental (solid line) and analytical (thin line) data: single porosity u160 (black circle), hybrid configuration with double porosity u160 in front and heterogeneous u160-melamine on the back (black triangle), hybrid configuration in vice versa (inversed black triangle).

The validity of this criterion is confirmed by Tarnow paper [18], where the geometrical expression of equation (24) is calculated. In [17], referring to the flux analogy, the boundary conditions are imposed on a circular cell, with equivalent area, because the direct analytical integration does not exist for the case of a square cell. The results shown in this Section confirm that this choice represent a good approximation. Additional details are discussed in the conclusions. For configurations A and B, there is a good agreement between experimental data and analytical prediction (Figure 17 and 18), provided that the diffusion function F_d is set to 1. On the other hand, the prediction is worse when the complete expression for F_d, equation (18), is taken into account. These considerations are valid for both cases of double porosity and melamine inclusions. Physically, the diffusion effect is not well represented in the Small Kundt Tube. This fact can be explained by the following reasons:

- the layer is not periodic as in the Big Kundt Tube, but only one cell is considered, therefore one of the hypotheses of the homogenization theory is not respected;
- the external cross section is circular and not square, thus enlarging the difference between the real sample and an ideal periodic layer;
- in all the experimental cases, the separation between micro and meso scales is sufficient to satisfy the second homogenization hypothesis [3] that imposes at least $l_m/l_p < 10^{-1}$ (Table VI), but the permeability contrast in some cases is not high enough.

The last explanation is more clear if the description in [3] is considered: for $l_m/l_p \approx 10^{-1}$, there is a low static permeability contrast between pores and micropores; for $l_m/l_p \approx 10^{-3}$, there is a high static permeability contrast. Table VI shows that the first situation occurs clearly in the Big Kundt Tube; in the Small Kundt Tube, two different situations must be considered, due to the value of l_m/l_p that is not a priori clearly referable to one of the two situations. For configurations A and B (small perforation and inclusion), l_m/l_p is closer to the order 10^{-1}: in fact the prediction with $F_d = 1$ is good (Figure 17). Moreover, the diffusion effect appears to be more consistent when the internal cross-section is enlarged (configurations C and D, Figure 8). In this case, the separation of scales between micro and meso is more clear and the diffusion effect appears, due to the larger contact surface between u160 and melamine (or between u160 and air). The analytical predictions are satisfactory if the complete expression for F_d is considered.

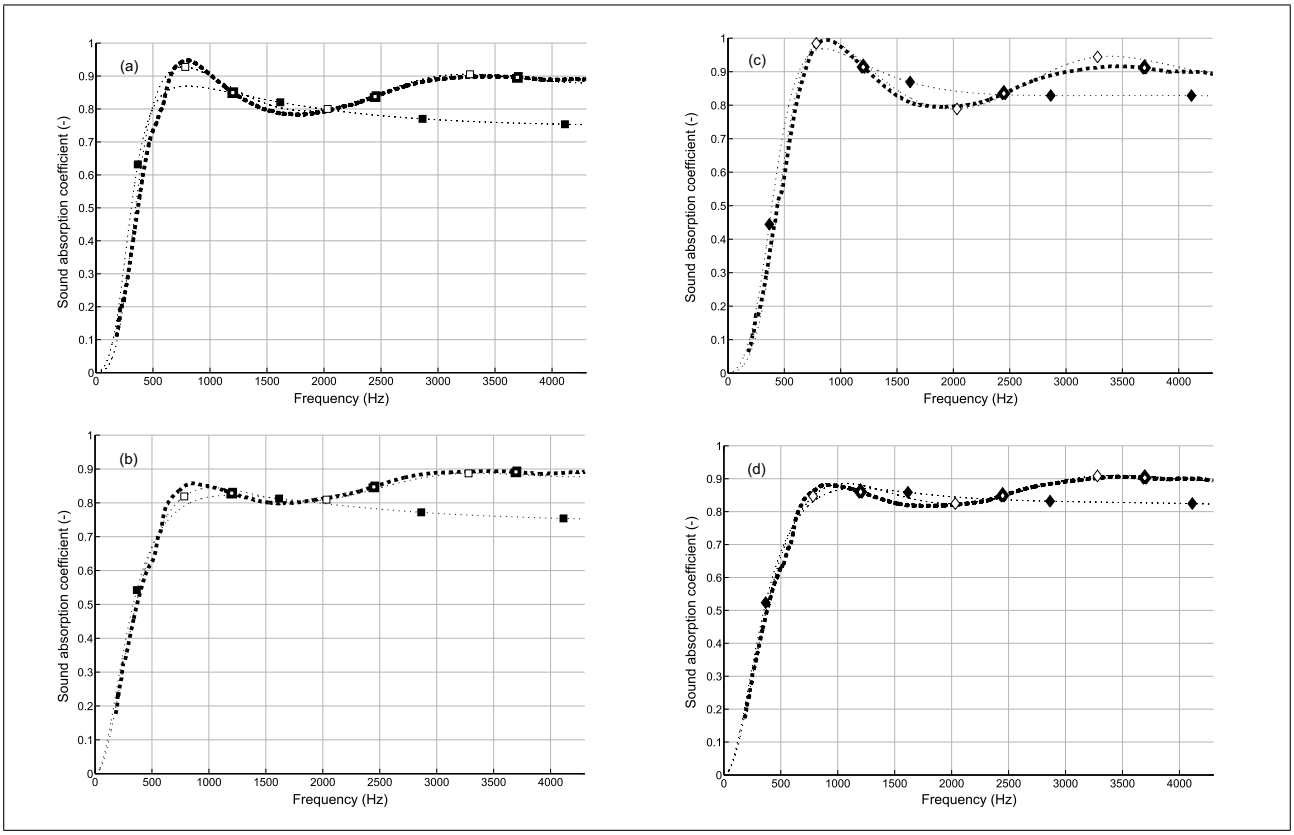


Figure 17. Small Kundt Tube, 45 mm thick layer, validation for configurations A and B. (a) Configuration A, double porosity: comparison between experimental data (thick black square) and anaytical model in case of $F_d = 1$ (thin black square) and $F_d = F_d(\omega)$ (thin black filled square). (b) Configuration A, heterogeneous material: comparison between experimental data (thick black square) and anaytical model in case of $F_d = 1$ (thin black square) and $F_d = F_d(\omega)$ (thin black filled square). (c) Configuration B, double porosity: comparison between experimental data (thick black diamond) and anaytical model in case of $F_d = 1$ (thin black diamond) and $F_d = F_d(\omega)$ (thin black filled diamond). (d) Configuration B, heterogeneous material: comparison between experimental data (thick black diamond) and anaytical model in case of $F_d = 1$ (thin black diamond) and $F_d = F_d(\omega)$ (thin black filled diamond).

The prediction of a high/low static permeability contrast, that is here evaluated through theoretical observations, will be confirmed in a further paper by the numerical calculations. In fact, a FEM model is a closer representation of the reality from this point of view, because the diffusion effect is a direct consequence of the geometrical modeling.

Another estimation of the diffusion effect is given by the wavelength in the microporous material. The key point in the case of high permeability contrast, is that the wavelength in the microporous domain is of the same order of magnitude as the mesoheterogeneities [3]. The situation is depicted in Figure 19: with this criterion in the case of the Big Kundt Tube, the diffusion effect is expected already at low frequencies. On the other hand, in the Small Kundt Tube the criterion gives similar results to the analysis of the ratio l_m/l_p. For configurations A and B an eventual diffusion effect would exist only at higher frequencies in the range of interest; enlarging the mesoheterogeneities size, the diffusion can arise at lower frequencies.

In conclusion, even if the periodicity hypothesis is not verified for a single circular-shaped cell, the semi-phenomenological model gives a good prediction, provided that the physical conditions of the experiment are taken into account. The experimental analysis in the Small Kundt Tube showed anyhow interesting results, when a comparison between different configurations is done, involving different geometrical sizes and single porosity/double porosity/heterogeneous case. The geometrical conditions must be analyzed very carefully when a semi-phenomenological model is concerned, especially about the involvement of the pressure diffusion effects. For a real application, it is strongly suggested to verify in the Big Kundt Tube the data obtained in the Small Kundt Tube, because in the latter the physical hypotheses of the homogenization theory are not guaranteed.

3.3.3. Single cell in the Medium Kundt Tube

The effect described in the previous section is confirmed by the experimental/analytical comparison in the Medium Kundt Tube (Figures 20 and 21). The analytical calculation refers to the case of a square-shaped (configurations A, B, C from Table III) or circularshaped (configuration D in Table III) perforation or inclusion into a circular-shaped cell.

For configurations A, B and D, it is not possible to define a clear situation between low or high permeability contrast. In fact, as shown by Table VI, the ratio l_m/l_p is

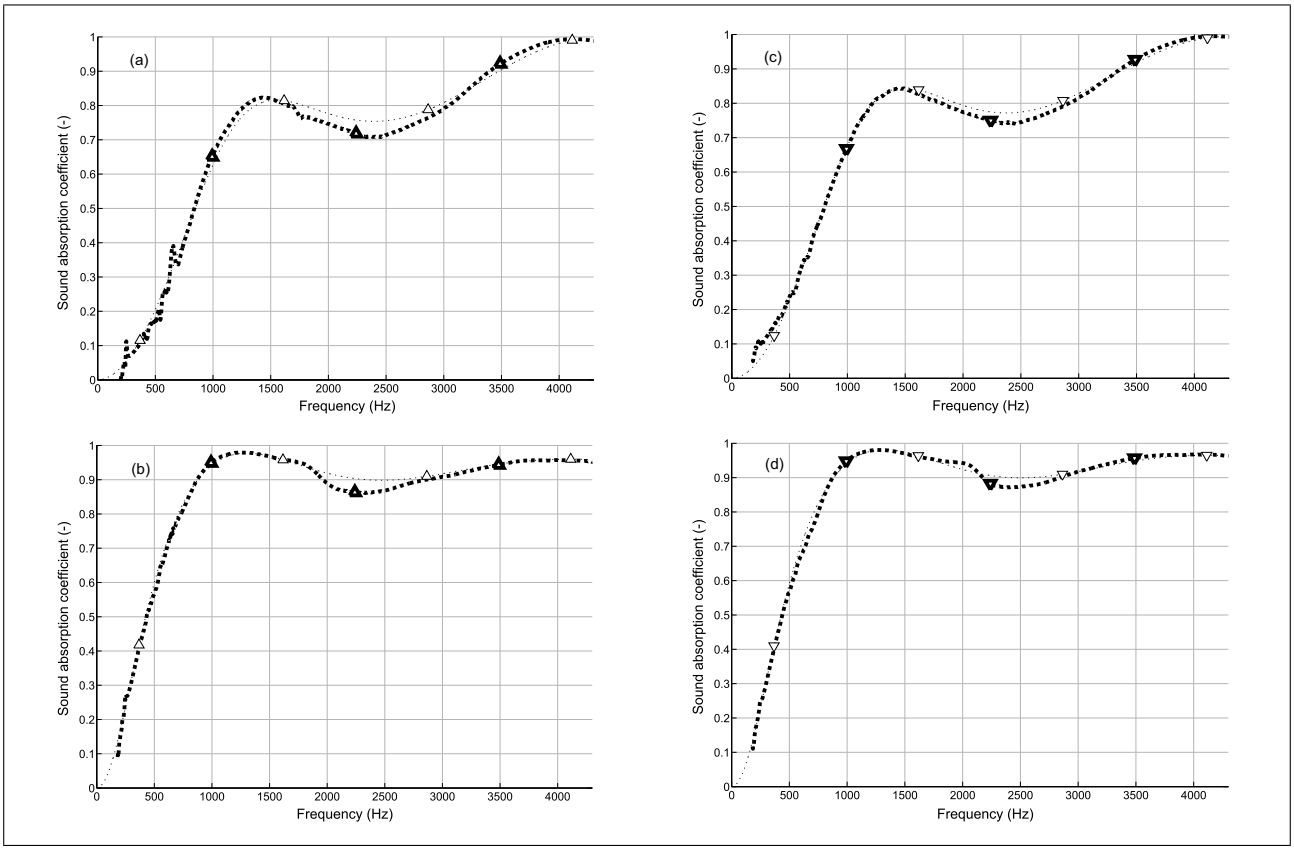


Figure 18. Small Kundt Tube, 45 mm thick layer, validation for configurations C and D. (a) Configuration C, double porosity: comparison between experimental data (thick black triangle) and anaytical model in case of $F_d = F_d(\omega)$ (thin black triangle). (b) Configuration C, heterogeneous material: comparison between experimental data (inversed thick black triangle) and anaytical model in case of $F_d = F_d(\omega)$ (inversed thin black triangle). (c) Configuration D, double porosity: comparison between experimental data (inversed thick black triangle) and anaytical model in case of $F_d = F_d(\omega)$ (inversed thin black triangle). (d) Configuration D, heterogeneous material: comparison between experimental data (inversed thick black triangle) and anaytical model in case of $F_d = F_d(\omega)$ (inversed thin black triangle).

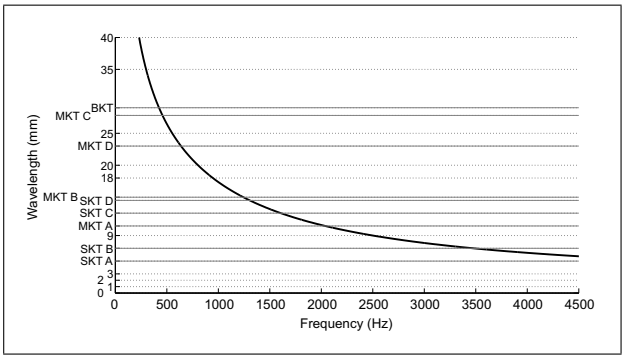


Figure 19. Wavelength in the u160 (rigid frame model) compared with the size of mesoheterogeneities: SKT refers to Small Kundt Tube, MKT to Medium and BKT to Big; A-B-C-D represent the configurations described in Tables II and III.

always of the order of 10^{-2}. Especially for configurations A and B, the situation is between the two cases, as Figure 20 shows and resembles the case described by Olny [2]. The comparison between the wavelength in the microporous domain and the mesoheterogeneities size confirms that the diffusion should arise at the tested frequencies. There is a pressure diffusion effect, but with the calculated diffusion frequency ω_d (equation (16)) the analytical model does not provide a very good estimation. On the other hand, some diffusion is present because - differently than the configurations A and B in the Small Kundt Tube - the mesoporous dimensions are increased, the permeability contrast is not really low and considering $F_d = 1$ is not sufficient to provide a good estimation too. In this case, the model is not validated: we assume that the effective ω_d is not well estimated (this hypothesis seems to be a good one by checking numerical results and has to be explored in further studies).

An easier estimation can be obtained for configuration C, where the permeability contrast is higher and sufficient to show the modelized pressure diffusion effect, even if for double porosity the agreement is slightly worse (but in any case the best prediction can be obtained this way). In conclusion, the cases in the Big Kundt Tube can be faced easily with the general semi-phenomenological model. The homogenization hypotheses are respected. Referring to Figures 16, 17, 18, 20 and 21, Table VII provides a summary of the physical conditions to be considered in order to obtain a satisfactory match between an-

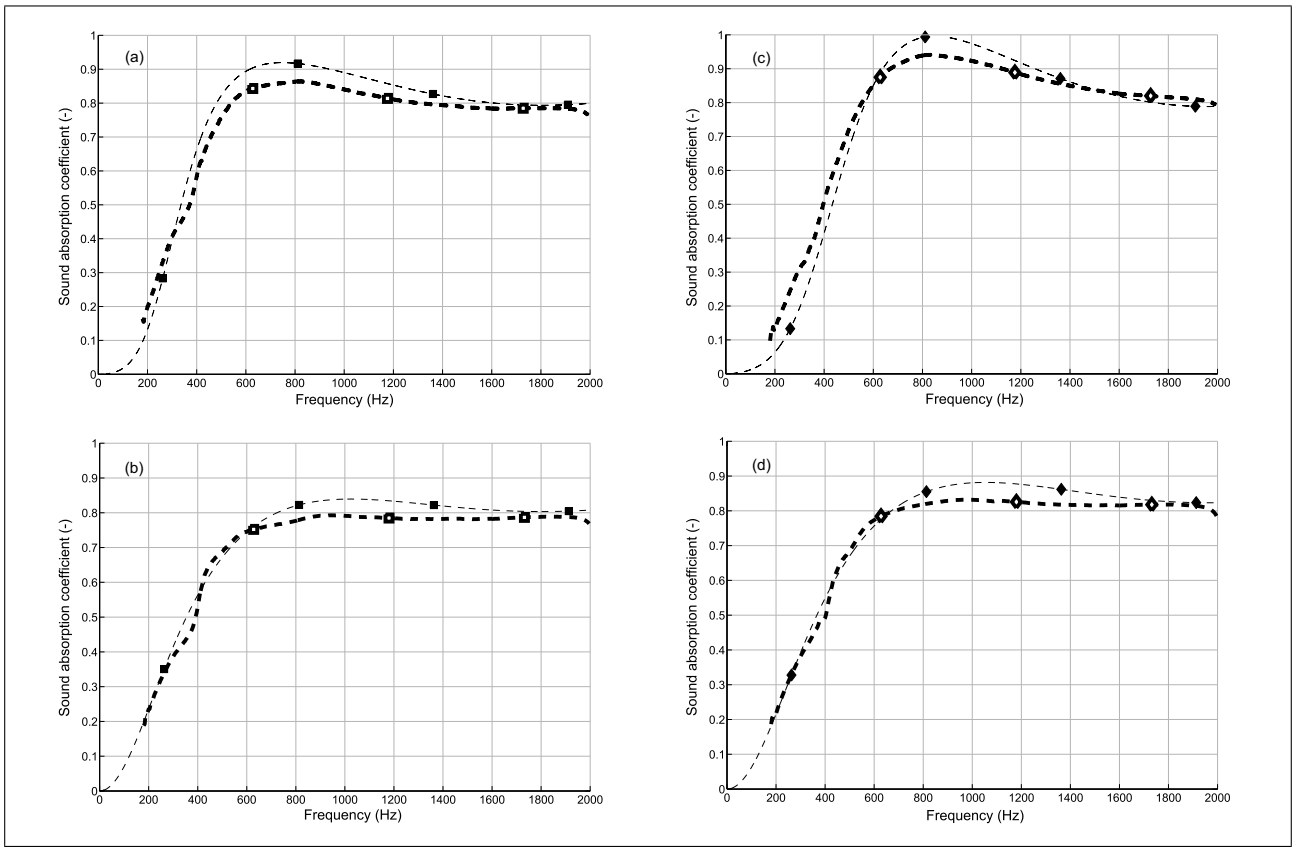


Figure 20. Medium Kundt Tube, 45.5 mm thick layer, validation for configurations A and B. (a) Configuration A, double porosity: comparison between experimental data (thick black square) and anaytical model in case of $F_d = 1$ (thin black filled square). (b) Configuration A, heterogeneous material: comparison between experimental data (thick black square) and anaytical model in case of $F_d = 1$ (thin black filled square). (c) Configuration B, double porosity: comparison between experimental data (thick black diamond) and anaytical model in case of $F_d = 1$ (thin black filled diamond). (d) Configuration B, heterogeneous material: comparison between experimental data (thick black diamond) and anaytical model in case of $F_d = 1$ (thin black filled diamond).

Table VII. Homogenization conditions and diffusion function for the different tested samples.

Kundt Tube type	Configuration	Permeability contrast	Diffusion frequency $f_d = \omega_d/2\pi$ (Hz)	Diffusion function	Diffusion frequency well estimated
Big Kundt Tube	6×6 cells	HIGH	1070	$F_d = F_d(\omega)$	YES
Small Kundt Tube	A	LOW	1868	$F_d = 1$	YES
Small Kundt Tube	B	LOW	2891	$F_d = 1$	YES
Small Kundt Tube	C	HIGH	11118	$F_d = F_d(\omega)$	YES
Small Kundt Tube	D	HIGH	12348	$F_d = F_d(\omega)$	YES
Medium Kundt Tube	A	LOW/HIGH	381	$F_d = F_d(\omega)$	NO
Medium Kundt Tube	B	LOW/HIGH	598	$F_d = F_d(\omega)$	NO
Medium Kundt Tube	C	HIGH	2546	$F_d = F_d(\omega)$	YES
Medium Kundt Tube	D	LOW/HIGH	1044	$F_d = F_d(\omega)$	NO

alytical prediction and experimental data. The separation between high and low permeability contrast is not obvious in some cases, but a general trend can be predicted when the interscale ratio is taken into account. This criterion is confirmed by the curves provided in the different figures: for low permeability contrast the diffusion function has to be fixed to 1, and for high permeability contrast it has to follow the complete semi-phenomenological model, in order to get a good prediction. The behavior of some samples in the Medium Kundt Tube for which the situation is not clear require to have a better estimation for the diffusion function.

3.3.4. Periodical cells in the Big Kundt Tube - case of rockwool

In this case the semi-phenomenological model described in a previous part has been used to predict the sound absorption coefficient for the configurations tested in the Big Kundt Tube, with rockwool as microporous material acting as a frame.

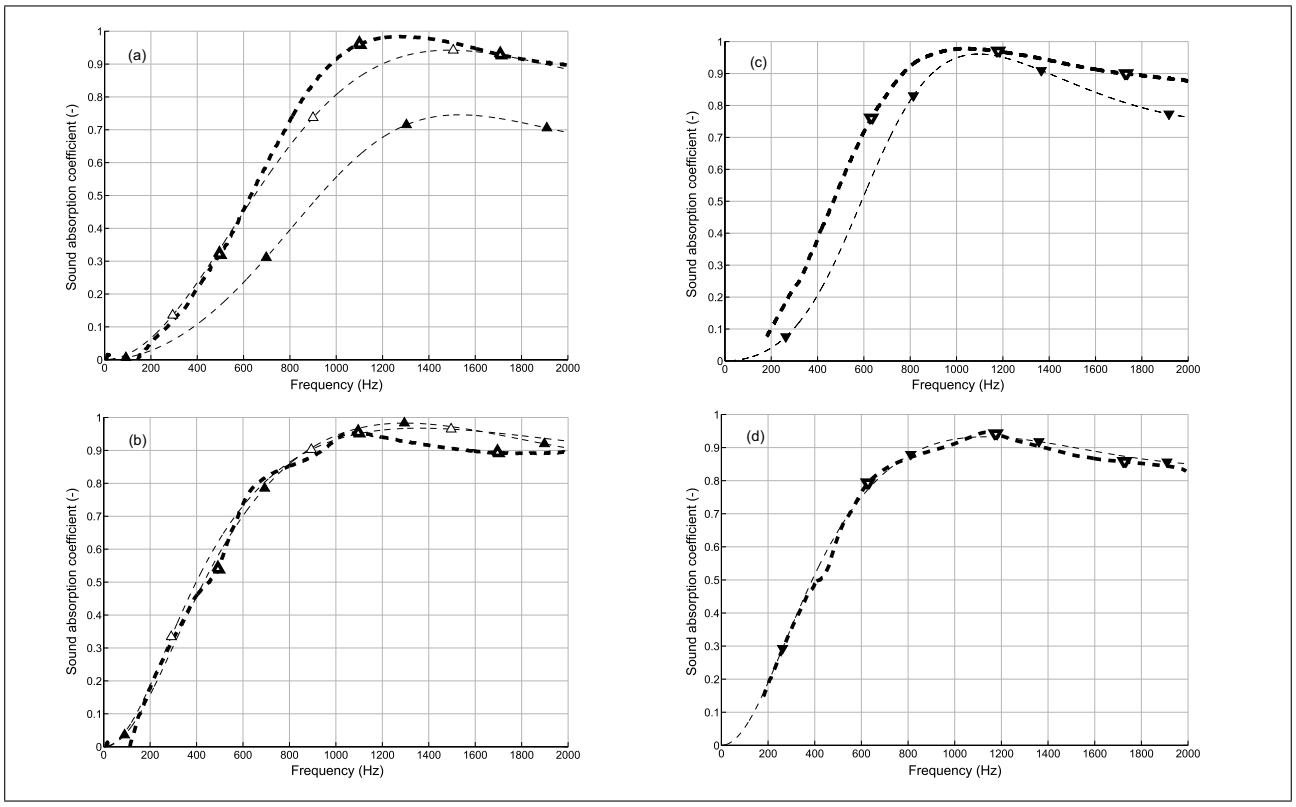


Figure 21. Medium Kundt Tube, 45.5 mm thick layer, validation for configurations C and D. (a) Configuration C, double porosity: comparison between experimental data (thick black triangle) and anaytical model in case of $F_d = F_d(\omega)$ (thin black triangle) and $F_d = 1$ (thin black filled triangle). (b) Configuration C, heterogeneous material: comparison between experimental data (thick black triangle) and anaytical model in case of $F_d = F_d(\omega)$ (thin black triangle) and $F_d = 1$ (thin black filled triangle). (c) Configuration D, double porosity: comparison between experimental data (thick black inversed triangle) and anaytical model in case of $F_d = F_d(\omega)$ (thin black filled inversed triangle) from which $f_d = 1044$ Hz. (d) Configuration D, heterogeneous material: comparison between experimental data (thick black inversed triangle) and anaytical model in case of $F_d = F_d(\omega)$ (thin black filled inversed triangle) from which $f_d = 1044$ Hz.

The results underlined in a previous section are confirmed (Figure 22): there is a good agreement between experimental data and analytical prediction, since the homogenization hypotheses are represented with a good approximation in the experimental data by the presence of a 6×6 and 7×7 networks of cells. The semi-phenomenological model provides a good comparison for all the configurations considered: 6×6 and 7×7, double porosity and heterogeneous material, two hybrid solutions.

As in case of u160, the small difference between the analytical and the experimental curves in Figure 22 can be ascribed to the axial tolerance of the perforations. Some small gaps of air between the layers can lead also to this effect (as already underlined in a previous section, when comparing the flexibility of rockwool to the one of u160), giving a slight overestimation of the experimental absorption curve.

As in case of u160, the intersections between predicted curves are approximately at the same frequencies as the corresponding intersections between experimental curves: the semi-phenomenological model gives a good prediction when a comparison is done between different curves (e.g. cases of optimization).

4. Conclusions

The semi-phenomenological model has been validated and has provided in general good agreement with the experimental results, for both cases of double porosity and in particular of specific heterogeneous inclusion. The results show that it is possible to extend the double porosity model to inclusions: the modified version of the double porosity model for heterogeneities with specific inclusions can be used with success, with the same characteristics and limits of the original double porosity model. For both cases, care must be taken about the physical interpretation of the pressure diffusion effects. In particular, it is important to verify: if the homogenization hypotheses are respected (periodicity and micro/meso/macro characteristic sizes) and how the permeability contrast is (high or low), through the analysis of the micro and meso dimensions, the analysis of the micro wavelength and the analysis of the diffusion frequency.

In some cases, as described in previous Sections, the pressure diffusion effects are not well estimated. It would be important to have a better prediction of the effective behavior of the pressure in the system.

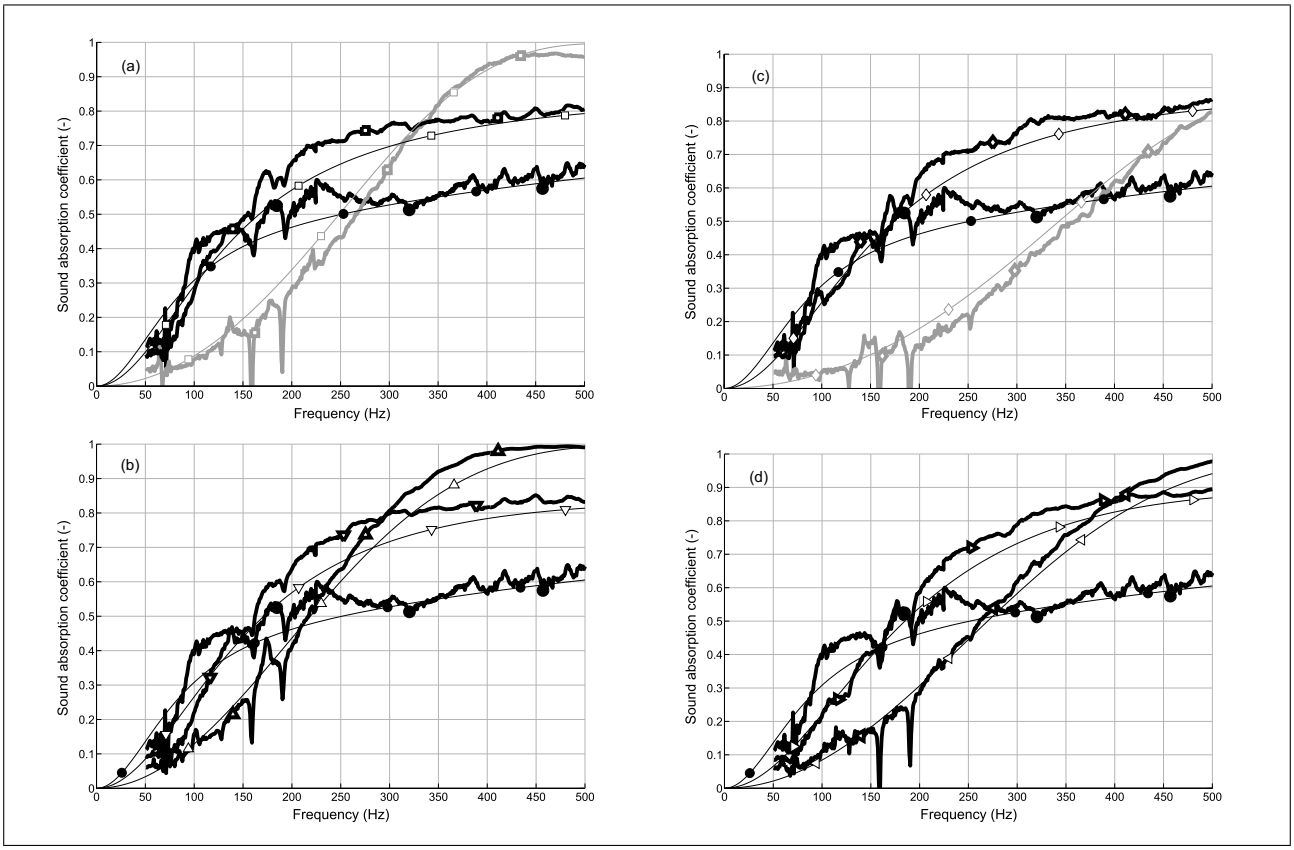


Figure 22. Big Kundt Tube, 90 mm thick layer composed of rockwool and melamine, validation. (a) 6 x 6 periodical cells, comparison between experimental (solid line) and analytical (thin line) data: single porosity rockwool (black circle), double porosity rockwool (grey square), heterogeneous rockwool-melamine (black square). (b) 6 x 6 periodical cells, comparison between experimental (solid line) and analytical (thin line) data: single porosity rockwool (black circle), hybrid configuration with double porosity rockwool in front and heterogeneous rockwool-melamine on the back (black triangle), hybrid configuration in vice versa (inversed black triangle). (c) 7 x 7 periodical cells, comparison between experimental (solid line) and analytical (thin line) data: single porosity rockwool (black circle), double porosity rockwool (grey diamond), heterogeneous rockwool-melamine (black diamond). (d) 7 x 7 periodical cells, comparison between experimental (solid line) and analytical (thin line) data: single porosity rockwool (black circle), hybrid configuration with double porosity rockwool in front and heterogeneous rockwool-melamine on the back (black triangle -<-), hybrid configuration in vice versa (inversed black triangle ->-).

Some trials have already been done, in order to calculate an analytical value of $D(0)$ for different cross-sections (geometries more complicated than the square-circular case), but with no success. A simple investigation should be interesting. Using the flux analogy, a FEM calculation should be performed to obtain numerically the value of $D(0)$. Extending this concept, the calculation could be performed for several geometries and dimensions, in order to create a simple abacus for $D(0)$. Also for this reason, the numerical calculation described in a next paper will provide important information.

However, when the physical hypotheses are fully respected, the model is in agreement with experimental measurements (BKT). In other cases (SKT and MKT), the agreement is obtained provided that high/low permeability contrast and pressure diffusion frequency are taken into account: the model can give a first trend, which has to be confirmed by doing other experimental measurements which can respect the physical hypotheses (like the BKT).

To conclude, heterogeneous materials with inclusions provide the following advantages: an increase of sound absorption coefficient above a certain frequency due to diffusion effects; a smaller decrease of sound absorption coefficient at very low frequency compared with double porosity material and a better behavior in transmission compared with double porosity materials (to be discussed in details: see Appendix A).

Heterogeneous materials with specific inclusions represent a valid alternative to double porosity materials.

Further studies will involve, as well as all the aspects cited above, a numerical verification.

Acknowledgements

This work has been developed within the Laboratory INTERMECH (Laboratorio per la meccanica avanzata), of the network Rete Alta Tecnologia of Regione Emilia Romagna. The authors thank DGCB-ENTPE for the use of the experimental devices.

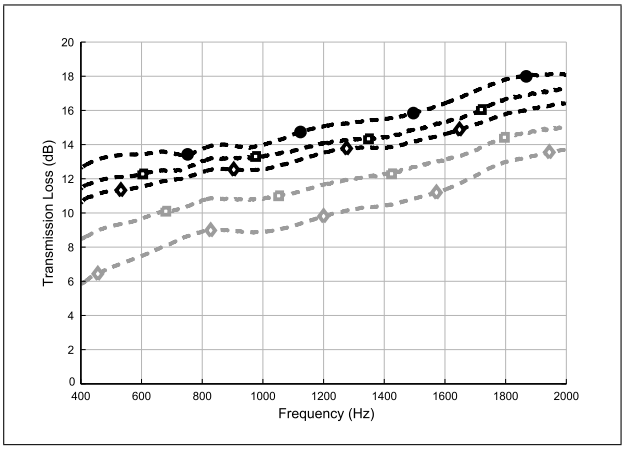


Figure A1. Medium Kundt Tube, measured TL comparison between single porosity u160 (black circle), double porosity u160 for configurations A (grey square) and B (grey diamond) and u160 with inclusions of melamine for configurations A (black circle) and B (black diamond).

Appendix

A1. Example of Transmission Loss Measurements

Transmission Loss has been measured for some configurations described in previous sections. The measurement has been done in the Medium Kundt Tube, using an anechoic termination. The experimental data presented in Figure A1 refer to configurations A and B of Table III, with u160 as frame microporous material and melamine for the inclusions (Table I). When the mesoporosity is increased, performances in transmission are decreased, however when the inclusion is concerned, the behavior is almost as good as for the single porosity material. For both cases, the TL is higher for the case of inclusions than the case of double porosity, for the whole frequency range.

In this case the sample is not backed by any plate; other configurations will be shown in a forthcoming paper.

References

[1] C. Boutin, P. Royer, J.-L. Auriault: Acoustic absorption of porous surfacing with dual porosity. Special Issue on poroelasticity - International Journal of Solids and Structures **35** (1998) 4709–4737.

[2] X. Olny: Acoustic absorption of porous media with single and double porosity-modeling and experimental solution (in french). Ph.D. thesis - ENTPE-Institut National des Sciences Appliquées de Lyon (1999).

[3] X. Olny, C. Boutin: Acoustic wave propagation in double porosity media. J. Acoust. Soc. Am. **114** (2003) 73–89.

[4] N. Atalla, R. Panetton, F. Sgard, X. Olny: Acoustic absorption of macro-perforated porous materials. J. Sound Vib. **243** (2001) 659–678.

[5] F. Sgard, X. Olny, N. Atalla, F. Castel: On the use of perforations to improve the sound absorption of porous materials. Appl. Acoustics **66** (2005) 625–651.

[6] F. Sgard, N. Atalla, C. Amedin: Vibro-acoustic behavior of a cavity backed by a plate coated with a meso-heterogeneous porous material. Acta Acustica United with Acustica **93** (2007) 106–114.

[7] N. Atalla, F. S. et al: Etude numérique et expérimentale de l'absorption acoustique et de la transparence acoustique des matériaux poreux hétérogènes en basses fréquences dans le but d'identifier des solutions à fort potentiel d'applicabilité. Rapport final de recherche présenté à l'IRSST **GAUS, Département de Génie Mécanique, Université de Sherbrooke** (Octobre 2001) R–278.

[8] N. Atalla, F. S. et al: Développement de nouveaux matériaux absorbants à hautes performances acoustiques pour diminuer le bruit en basses fréquences. Rapport final de recherche présenté à l'IRSST **GAUS, Département de Génie Mécanique, Université de Sherbrooke** (Septembre 2003) R–370.

[9] N. Amirouche: Dispositifs absorbants à base de matériaux à double porosité dans des champs acoustiques complexes. Ph.D. thesis - Entpe - France (2008).

[10] K. Horoshenkov: Innovative applications of materials for acoustic purposes. Appl. Acoustics **66** (2005) 603–605.

[11] G. Pispola, K. Horoshenkov, A. Khan: Comparison of two modeling approaches for highly heterogeneous porous media. J. Acoust. Soc. Am. **121** (2007) 961–966.

[12] L. D. Ryck, J. Groby, P. Leclaire, W. Lauriks, A. Wirgin, C. Depollier, Z. Fellah: Acoustic wave propagation in a macroscopically inhomogeneous porous medium saturated by a fluid. Appl. Phys. Lett. **90** (2007) 181901.

[13] J.-P. Groby, A. Wirgin, L. D. Ryck, W. Lauriks: Acoustic response of a rigid frame porous medium slab with a periodic set of inclusions. J. Sound Vib. **arXiv:0705.2754v1** (2007).

[14] E. Gourdon, M. Seppi: On the use of porous inclusions to improve the acoustical response of porous materials: Analytical model and experimental verification. Applied Acoustics **71** (2010) 283–298.

[15] D. Johnson, J. Koplik, R. Dashen: Theory of dynamic permeability and tortuosity in fluid-saturated porous media. J. Fluid Mech. **176** (1987) 379–402.

[16] Y. Champoux, J.-F. Allard: Dynamic tortuosity and bulk modulus in air-sturated porous media. J. Appl. Phys. **70** (1991) 1975–9.

[17] D. Lafarge, P. Lemarinier, J.-F. Allard, V. Tarnow: Dynamic compressibility of air in porous structures at audible frequencies. J. Acoust. Soc. Am. **102** (1997) 1995–2006.

[18] V. Tarnow: Airflow resistivity of models of fibrous acoustic materials. J. Acoust. Soc. Am. **100** (1996) 3706–3713.

[19] L. Beranek: Acoustic impedance of porous materials. J. Acoust. Soc. Am. **13** (1942) 248–260.

[20] A. C-522: Standard test method for airflow resistance of acoustical materials. American Society for Testing and Materials (2003).

[21] X. Olny, R. Panneton, J. Tran-Van: An indirect acoustical method for determining intrinsic parameters of porous materials. Proc. of the Second Biot Conference on Poromechanics (2002).

[22] C. Langlois, R. Panneton, N. Atalla: Polynomial relations for quasi-static mechanical characterization of isotropic poroelastic materials. J. Acoust. Soc. Am. **110** (2001) 3032–3040.

[23] R. Lanoye: Assessment of the absorption performance of sound absorbing materials: use of the trefftz's method and of a new dual particle velocity-pressure sensor. Ph.D. thesis - Katholieke Universiteit Leuven (2007).